Journal of Structural Geology, Vol. 14, No. 7, pp. 873 to 885, 1992
Printed in Great Britain

0191-8141/92 $05.00+0.00

Laboratory testing of an automatic method for determining normal fault geometry at depth

HUGH G. KERR and NICKY WHITE

Bullard Laboratories, University of Cambridge, Madingley Road, Cambridge CB3 OEZ, U.K.

(*Received* 2 *September* 1991; *accepted in revised form* 9 *March* 1992)

Abstract—A general kinematic method for determining two-dimensional normal fault geometries from a large number of hanging wall horizons has been tested on synthetic data and laboratory models. The method assumes that the hanging wall deforms by a combination of arbitrarily inclined bulk simple shear and differential compaction. It should be applicable to normal faults which do not change shape as deformation proceeds. Fault geometry, the inclination of simple shear and compaction parameters may all be uniquely determined provided that the geometry of the hanging wall stratigraphy is accurately known prior to and after deformation. Testing the method on synthetic data has shown that unique solutions can be found. Solutions obtained using large numbers of hanging wall horizons of laboratory-modelled faults are encouraging: in each case the method was able to predict a fault geometry close to the fault geometry used in the laboratory model. Hence bulk simple shear appears to be a good approximation of hanging wall deformation. The inclination of simple shear appears to be controlled by the underlying fault geometry rather than the amount of extension or the composition of the hanging wall fill. In future, it is hoped that a general method similar to this one can be applied routinely to depth-converted seismic reflection data.

INTRODUCTION

KNOWLEDGE of the geometry of normal faults at depth is of importance both to academics and to the oil industry. On seismic reflection sections, it is often possible to image clearly the beds within a fault block but not the fault surface itself. In this paper we extensively test a kinematic method which relates the geometry of the fault surface to the geometry of the observed beds.

Over the last 10 years a large number of kinematic models have been suggested. These kinematic models fall into three broad categories: (a) shear models (Verrall 1981, Gibbs 1983, Jackson & Galloway 1984, Kligfield *et al.* 1984, White *et al.* 1986, Faure & Chermette 1989, Groshong 1990, Nunns 1991); (b) flexural-slip models (Suppe 1983, Davison 1986, Rowan & Kligfield 1989, Higgs *et al.* 1991); and (c) constant-slip models (Williams & Vann 1987). All of these models are two-dimensional (i.e. they assume that deformation occurs within the plane of the section). White & Yielding (1991) have suggested that the existence of such large numbers of models is unsatisfactory; it would be much better if there was just one model that could be applied in all cases rather than having to decide which model is applicable in each individual case.

White & Yielding (1991) conclude that the most applicable method is the simple shear model. Roberts *et al.* (1990) have come to a similar conclusion, although they are particularly concerned that any such method should only be applied to small-scale surficial normal faulting. The simple shear model conserves mass, predicts faulting within the hanging wall, and can easily be modified to allow for compaction. Furthermore, the shear model can be used to solve both the forward and inverse problems (i.e. the geometry of the beds can be predicted from the fault and more importantly the geometry of the fault can be calculated from the observed beds).

At present, shear models assume that the hanging wall deforms by bulk simple shear which can be either vertical (Verrall 1981) or arbitrarily inclined (White *et al.* 1986). The best known shear model is the 'Chevron construction' (Verrall 1981) which assumes that the hanging wall deforms by vertical shear. Considering that vertical shear is a special case of arbitrarily inclined shear, it is clear that arbitrarily inclined shear is the more useful model. Hence White & Yielding (1991) have suggested on the basis of some preliminary results that the arbitrarily inclined bulk simple shear model can be used generally to determine fault geometry at depth.

The arbitrarily inclined simple shear model has been applied in the past to synthetic faults, laboratory-modelled faults, and real seismic examples (White 1987, 1992, White & Yielding 1991). It is now apparent that the inversion scheme used in this previous work was not entirely satisfactory. The original scheme was based on the minimization of the areal difference between faults predicted from each individual bed (White 1987). In this paper, we show that area is not the most useful measure of the difference between the predicted faults and instead we propose a more appropriate misfit function.

The main purpose of this paper is to test the revised scheme on synthetic data and more importantly to apply it to a large number of published laboratory-modelled faults (McClay & Ellis 1987, Ellis & McClay 1988). This paper is therefore a considerable expansion of White (1992), where some preliminary results of the original inversion scheme were presented.

THE METHOD

White *et al.* (1986) derived a generalized model for the deformation of beds within the hanging wall of a fault block. This model was subsequently revised by White (1987) to allow for large displacements. The main assumptions in both cases are that the fault remains the same shape throughout deformation, that the stratigraphy is known prior to and after deformation, and that the hanging wall deforms within the plane of the section by a combination of arbitrarily inclined bulk simple shear and differential compaction. A major constraint on the model is that solid area (i.e. the total area minus the integrated porosity) must be conserved during deformation. Compaction can then be calculated using an empirical relationship between porosity $\phi(z)$, and depth z (e.g. Sclater & Christie 1980):

$$\phi(z) = \phi_0 \exp(-z/\lambda), \quad (1)$$

where ϕ_0 is the initial porosity and λ the porosity decay length. Deformation of the hanging wall is consequently defined by three parameters: the angle of simple shear α, measured from vertical; and the two parameters related to compaction, ϕ_0 and λ. α is positive if the shear is antithetic in direction.

Ideally compaction should be modelled as occurring vertically. However this is not a simple problem to solve when combined with non-vertical simple shear (Waltham 1990). The simplest approximation is to constrain compaction to occur parallel to the direction of shear. This solution is most valid for α less than 45°.

The equation (White 1987) relating deformation of the hanging wall, by a combination of simple shear and differential compaction, to the geometry of the fault is (for a full derivation see White 1987, 1992):

$$\begin{aligned} F'(x'+h') = {} & F'(x') - R'(x') + B'(x'+h') \\ & + \phi_0'\lambda'\{\exp(-F'(x')/\lambda') \\ & - \exp(-R'(x')/\lambda') \\ & - \exp(-F'(x'+h')/\lambda') \\ & + \exp(-B'(x'+h')/\lambda')\}. \end{aligned} \quad (2)$$

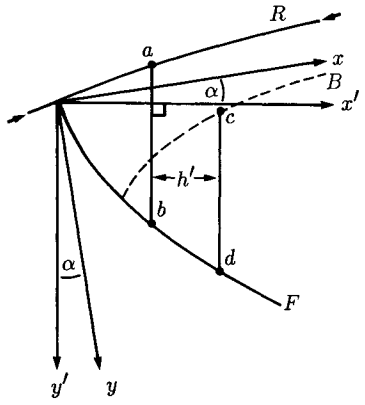

Fig. 1. Co-ordinate system and geometrical relationships used to derive equation (2). R is bed shape prior to extension (i.e. the regional). B is the geometry of deformed bed. In the rotated frame, $a = R'(x')$, $b = F'(x')$, $c = B'(x'+h')$ and $d = F'(x'+h')$. Solid lengths $|ab|$ and $|cd|$ are equal.

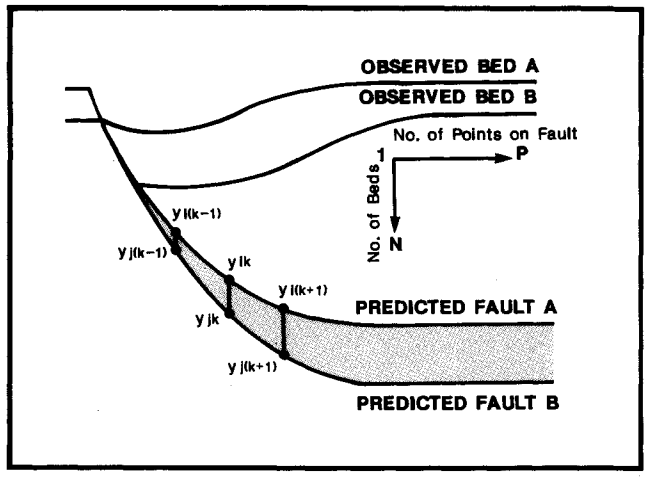

Fig. 2. The inverse problem: in general, for given values of α, ϕ_0 and λ, faults A and B can be calculated using beds A and B. To find correct fault geometry and correct values of α, ϕ_0 and λ, misfit function $\mathcal{M}$ between two calculated faults must be minimized by varying α, ϕ_0 and λ. P = number of points at which misfit is calculated. N = number of beds/faults. Misfit function evaluated by summing $(Y_{ik} - Y_{jk})$ for all pairs of calculated faults.

The reference frame x–y (Fig. 1), for all the co-ordinates, has been rotated from vertical clockwise through α, the angle of simple shear being considered, to reference frame x'–y'. $F'(x')$ and $B'(x')$ are the y' co-ordinates, at a point x', of the fault and bed, respectively, in the rotated frame. The variable h' is the heave, ϕ_0' is the initial porosity, λ' is the porosity decay length, and $R'(x')$ is the shape of the bed before deformation (i.e. the regional) all within the rotated frame. When the initial porosity (ϕ_0) is zero or the decay length (λ) is infinitely large, the equation reduces to a much simpler form which is equivalent to the beds deforming by simple shear alone without compaction

$$F'(x'+h') = F'(x' - R'(x') + B'(x'+h'). \quad (3)$$

Equation (2) may be solved by iteration in either the inverse problem for F when B is given or in the forward problem for B when F is given, provided the deformation parameters α, ϕ_0 and λ are set. Five iterations usually yield a solution accurate to several per cent. (White & Yielding 1991). Equation (3) provides the initial solution.

Unfortunately, in the inverse problem, the three parameters (α, ϕ_0 and λ) must all be known so that the correct fault geometry (F) may be calculated from a bed (B). In general only broad constraints may be placed on these three parameters.

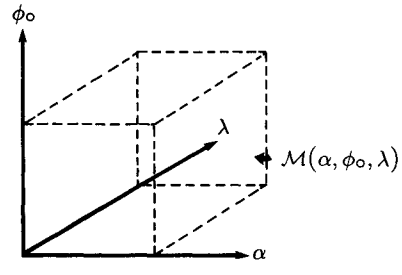

Fig. 3. Misfit function $\mathcal{M}$ is function of α, ϕ_0 and λ. Minimum value of $\mathcal{M}$ can be determined by systematically searching α–ϕ_0–λ space.

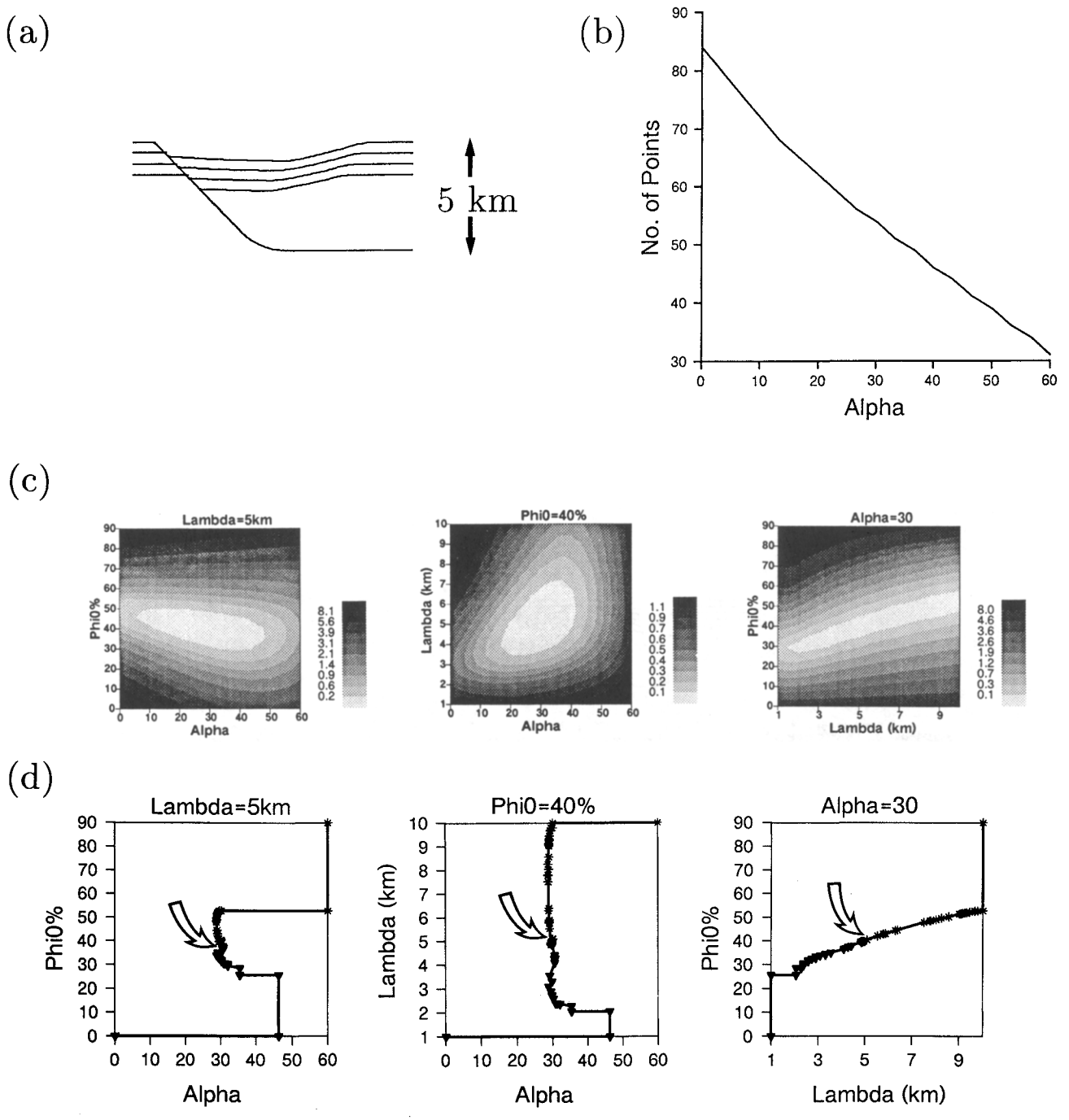

Fig. 4. (a) Synthetic model produced by forward modelling ($\alpha = 30°$, $\phi_o = 40\%$, $\lambda = 5$ km). Scale indicated at the right-hand-side of the model. (b) Plot of number of points P at which misfit is measured vs α. Note linear relationship. (c) shows three orthogonal plots of function $\mathcal{M}(\alpha,\phi_o,\lambda)$ positioned at known solution (see text). In each case, the correct solution (i.e. minimum value of $\mathcal{M}$) lies within the lightest shaded area. Contour interval indicated at the right-hand-side of each plot. The next figure organized in a similar fashion. (d) Same as (c) indicating the path taken of two arithmetic inversion runs using Powell's algorithm (see text and Press *et al.* 1986). Solid triangles indicate path from starting point at $\alpha = 0°$, $\phi_o = 0\%$ and $\lambda = 1$ km. Stars indicate path starting from $\alpha = 60°$, $\phi_o = 90\%$ and $\lambda = 10$ km. Arrows indicating method converges to correct solution from both starting points.

(1) α, the inclination of simple shear. Since we are concerned with an extensional system, α is unlikely to be less than 0°, as this would result in shortening within the hanging wall. Preliminary results suggest that α is also unlikely to be greater than 60° (White & Yielding 1991).

(2) ϕ_o, the initial porosity, cannot be less than 0% and is given an arbitrary upper limit of 90%.

(3) λ, the porosity decay length, for the main categories of sediment varies between 2 and 10 km (Sclater & Christie 1980).

Therefore, if the geometry of only one bed is known there is no unique solution to the problem. However, if the deformation parameters and the fault are common to all beds, all the unknowns including the fault geometry may be determined. The method employed to calculate the fault geometry is best explained by Fig. 2.

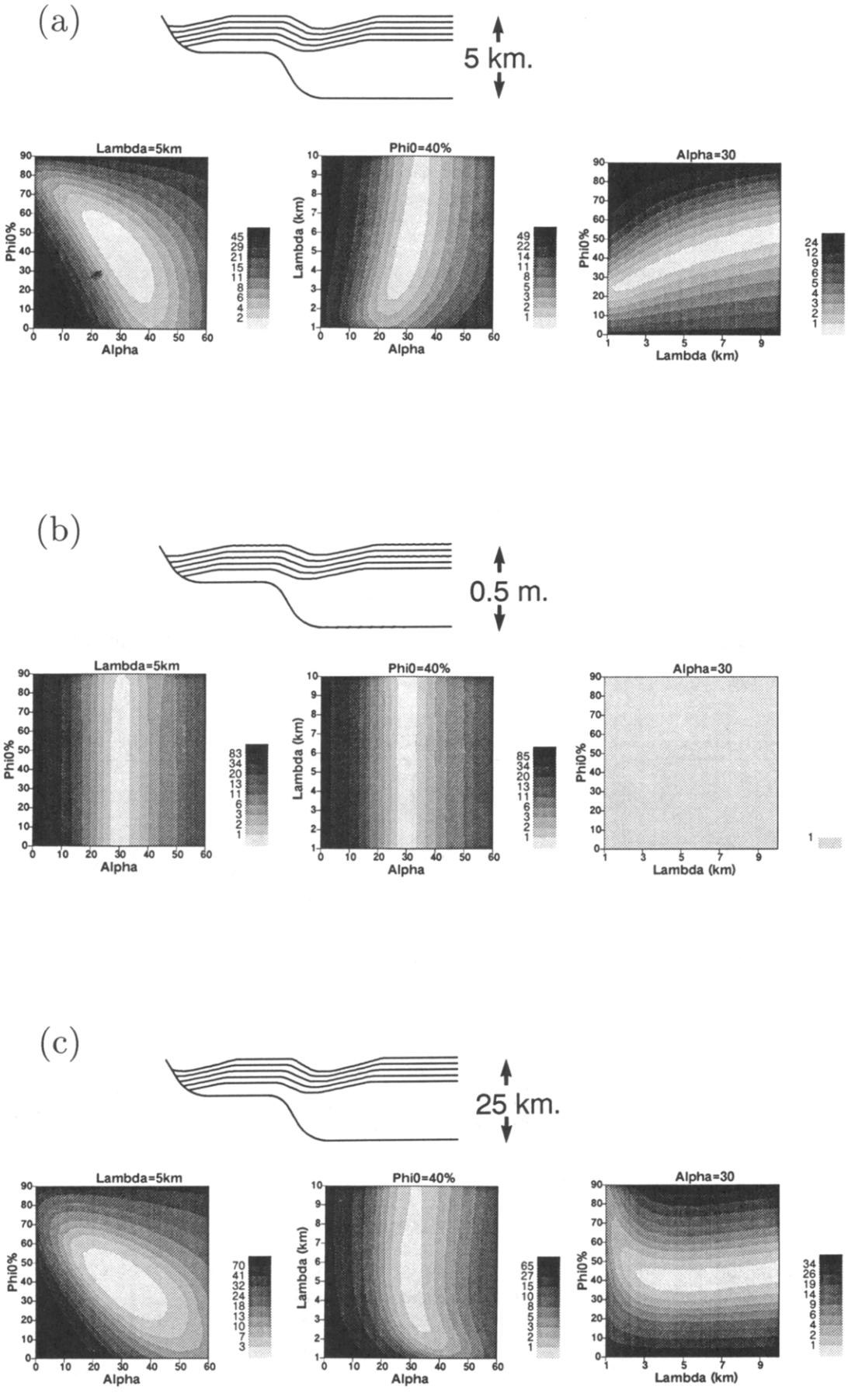

Fig. 5. Inverse modelling of three synthetic examples where fault shape stays the same (flat–ramp–flat) but the scale of the model changes (indicated at the right-hand-side of each model). In each case, $\alpha=30°$, $\phi_o=40\%$, $\lambda=5$ km. Note changes in shape of misfit function in each case.

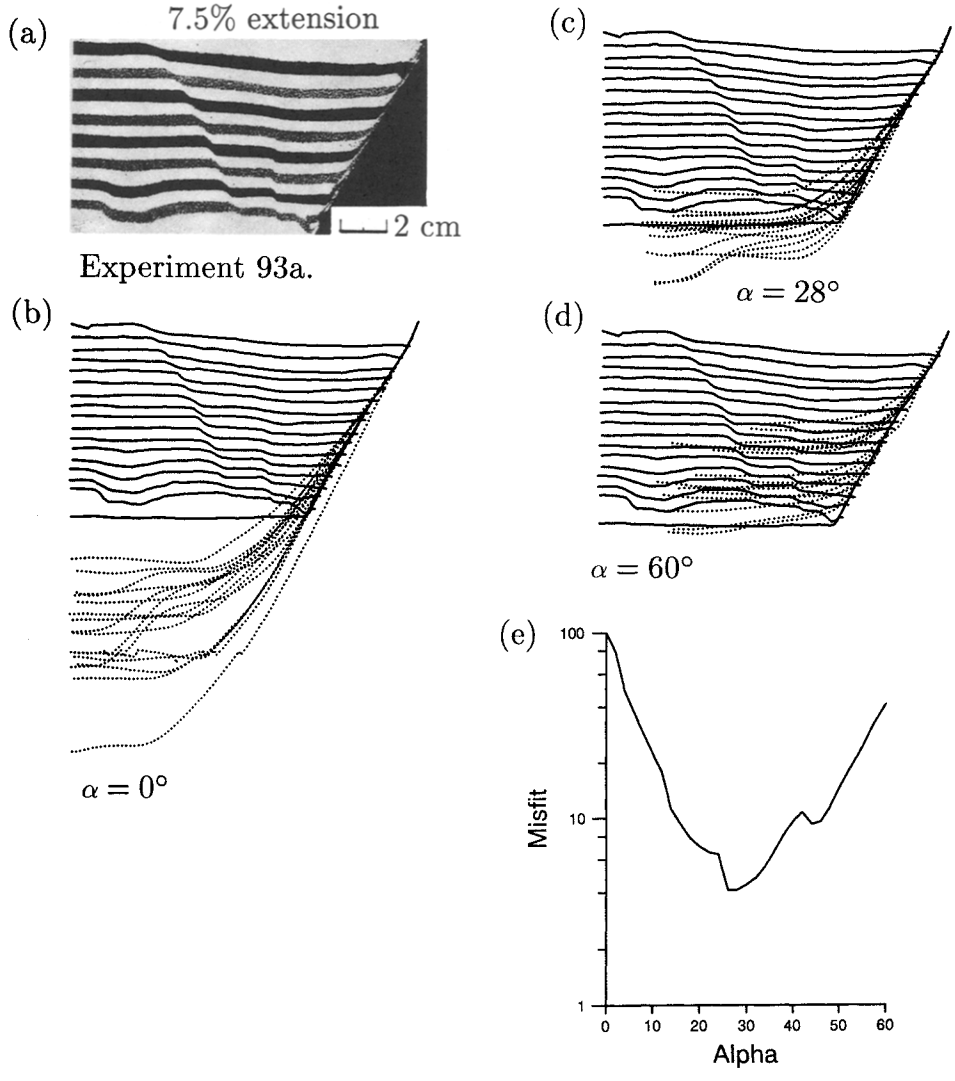

Fig. 6. (a) Dry sand-box model of normal fault (McClay & Ellis 1987, p. 118, fig. 5b. Experiment No. 93a, homogeneous sand layers). Reproduced with permission of Blackwell Scientific Publications Ltd. (b)–(d) Inverse models of (a) using geometry of 16 hanging wall horizons to determine fault geometry. Observed beds and fault; solid lines; calculated faults; dotted lines. Note best fit is example (c). (e) Plot of misfit function vs α. Note in this and subsequent examples misfit function normalized to 100 and plotted on logarithmic scale.

Here the same values of α, ϕ_o and λ, are used to predict fault A from bed A and fault B from bed B. If the predicted faults from each bed are the same (e.g. if fault A is the same as fault B), then, provided the assumptions regarding the deformation of the hanging wall are correct, the real fault will have been found. The inclusion of more than two beds yields more predicted faults and so increases confidence in the solution.

The original scheme used numerical integration to calculate the areal difference between the predicted faults within α–ϕ_o–λ space. When the areal difference is a mimimum it was concluded that the parameters defining the deformation of the hanging wall and the correct fault had been found. However, it is now apparent that although the idea of minimizing the difference between the predicted faults is a valid basis for an inversion scheme, area is not the most suitable measurement. Higher angles of shear result in the inversion scheme predicting shorter faults, the consequence of which, is that the areal difference is generally biased to smaller values at higher angles of shear. Instead of using area to compare the misfit between the sets of predicted faults, the distance in the y direction (i.e. vertical in the unrotated reference frame) between the predicted faults at every point along the section is now calculated, squared, summed, and divided by the number of points to give $\mathcal{M}(\alpha, \phi_o, \lambda)$, a measure of misfit,

$$\mathcal{M}(\alpha, \phi_o, \lambda) = \frac{1}{P}\left\{\sum_{i=1}^{N-1}\sum_{j=1+i}^{N}\sum_{k=1}^{P}(y_{ik} - y_{jk})^2\right\}, \quad (4)$$

where N is the number of imaged beds and P is the number of points at which the misfit is measured (Fig. 2). As we show in the next section, P is approximately a linear function of α, therefore $\mathcal{M}(\alpha, \phi_o, \lambda)$ is not affected by the length of the predicted fault and is a more appropriate method of comparing misfit at different values of α.

The revised inversion scheme is applied in a similar way to White (1987), the only difference being the calculation and minimization of misfit $\mathcal{M}(\alpha, \phi_o, \lambda)$ within α–ϕ_o–λ space (Fig. 3), instead of areal difference.

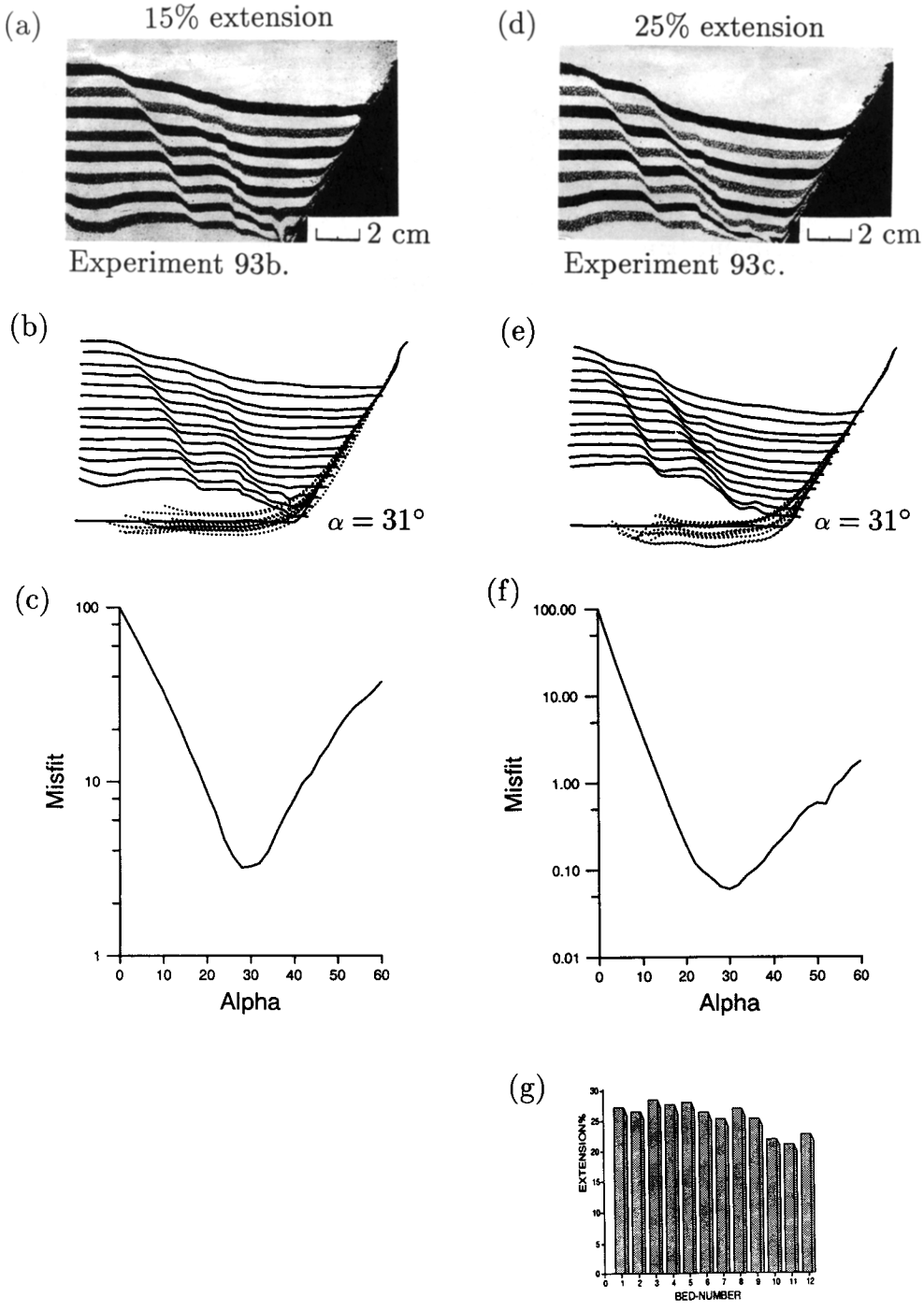

Fig. 7. (a) Dry sand-box model of normal fault (McClay & Ellis 1987, p. 118, fig. 5b. Experiment No. 93b, homogeneous sand layers). Reproduced with permission of Blackwell Scientific Publications Ltd. (b) inverse models of (a) using geometry of 14 hanging wall horizons. (c) Misfit function vs α. (d)–(f) same as before using sand-box model from McClay & Ellis (1987, p. 115, fig. 5c. Experiment No. 93c), homogeneous sand layers. Reproduced with permission of Blackwell Scientific Publications Ltd. Twelve beds used in inversion. (g) Calculated extension in per cent for each bed in (d).

TESTING THE INVERSION SCHEME

Before the inversion scheme can be applied generally it is necessary to establish the nature of function $\mathcal{M}(\alpha, \phi_o, \lambda)$ for different examples. Synthetic and laboratory-modelled faults in which both the geometries of the beds within the hanging wall and the fault geometry are known and where the assumption of two-dimensionality is valid provide an appropriate initial test.

SYNTHETIC FAULTS

The method used to generate the synthetic examples is demonstrated in Fig. 4. The forward model was first run to calculate beds from a defined fault shape (Fig. 4a), with the deformation parameters set at $\alpha = 30°$, $\phi_o = 40\%$ and $\lambda = 5$ km. The inverse model was then used to calculate misfit function $\mathcal{M}(\alpha, \phi_o, \lambda)$ within α–ϕ_o–λ space from the beds calculated by the forward

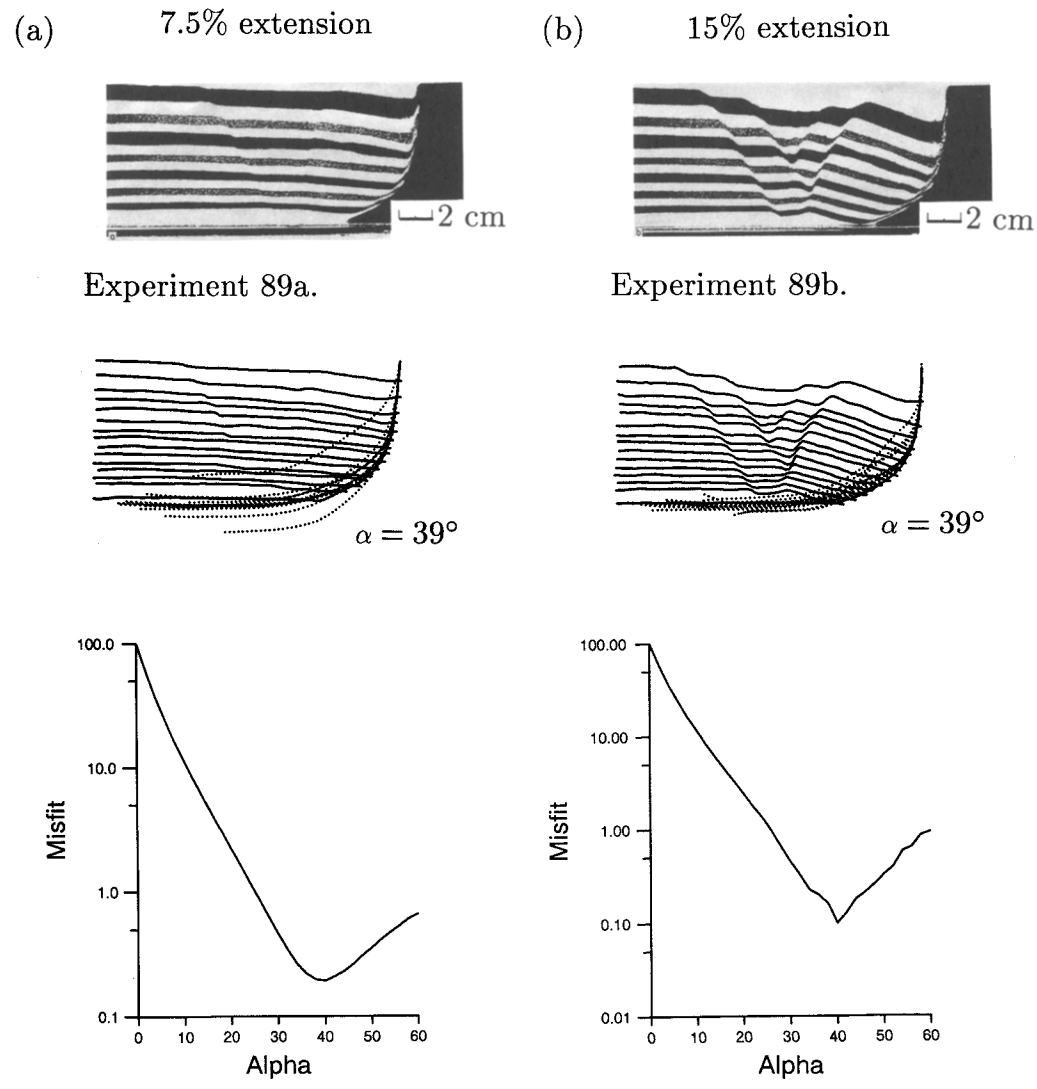

Fig. 8. (a) McClay & Ellis (1987, p. 121, fig. 6a. Experiment No. 89a) homogeneous sand layers. Reproduced with permission of Blackwell Scientific Publications Ltd. Inverse model and misfit function shown as before. Fourteen beds used. (b) McClay & Ellis (1987, p. 121, fig. 6b. Experiment No. 89b), homogeneous sand layers. Reproduced with permission of Blackwell Scientific Publications Ltd. Inverse model and misfit function shown as before. Fourteen beds used.

model. Figure 4(b) shows that there is an approximately linear relationship between α and P (the number of points at which misfit was measured). The linear relationship means that $\mathcal{M}(\alpha, \phi_o, \lambda)$ is a valid measure of the misfit between the predicted faults throughout α–ϕ_o–λ space. Resulting values of $\mathcal{M}(\alpha, \phi_o, \lambda)$ were contoured on three orthogonal sections located at the values of α, ϕ_o and λ used in the forward model (Fig. 4c). The contour plots give a good impression of the properties of the function. $\mathcal{M}(\alpha, \phi_o, \lambda)$ is a smooth function with a global minimum corresponding to values in running the forward model. The inverse and forward models are consequently self consistent. It is also apparent from the shape of the contours that α and ϕ_o are more significant than λ in constraining the minimum of the function.

The inversion scheme has been automated in order to find the global minimum of $\mathcal{M}(\alpha, \phi_o, \lambda)$ without having to sample α–ϕ_o–λ space completely. The method used was the modified Powell's method (Press *et al.* 1986). The method completes a number of successive line minimizations in a series of directions. The directions are governed by the average of the previous set of directions minus the direction in which the function made its largest decrease. The initial directions are set as the orthogonal unit vectors. Figure 4(d) illustrates the paths the method took through α–ϕ_o–λ space towards the global minimum (indicated by the arrow) when started from two different initial points for the example in Fig. 4(a). The star symbols indicate the path taken when the method was started at $\alpha = 60°$, $\phi_o = 90\%$ and $\lambda = 10$ km. Seventeen iterations were required to locate the minimum when started at this point. The solid triangles indicate the path taken when the method was started at $\alpha = 0°$, $\phi_o = 0\%$ and $\lambda = 1$ km: in this case 11 iterations were required to locate the minimum.

The model we use takes compaction into account and therefore it is important to apply the inversion to faults of different sizes to determine the sensitivity of $\mathcal{M}(\alpha, \phi_o, \lambda)$ to scale. In Fig. 5, three forward models using the same ramp–flat fault geometry at different scales are shown. In each case, the deformation parameters were set at $\alpha = 30\%$, $\phi_o = 40\%$ and $\lambda = 5$ km. Figure 5(a) is at

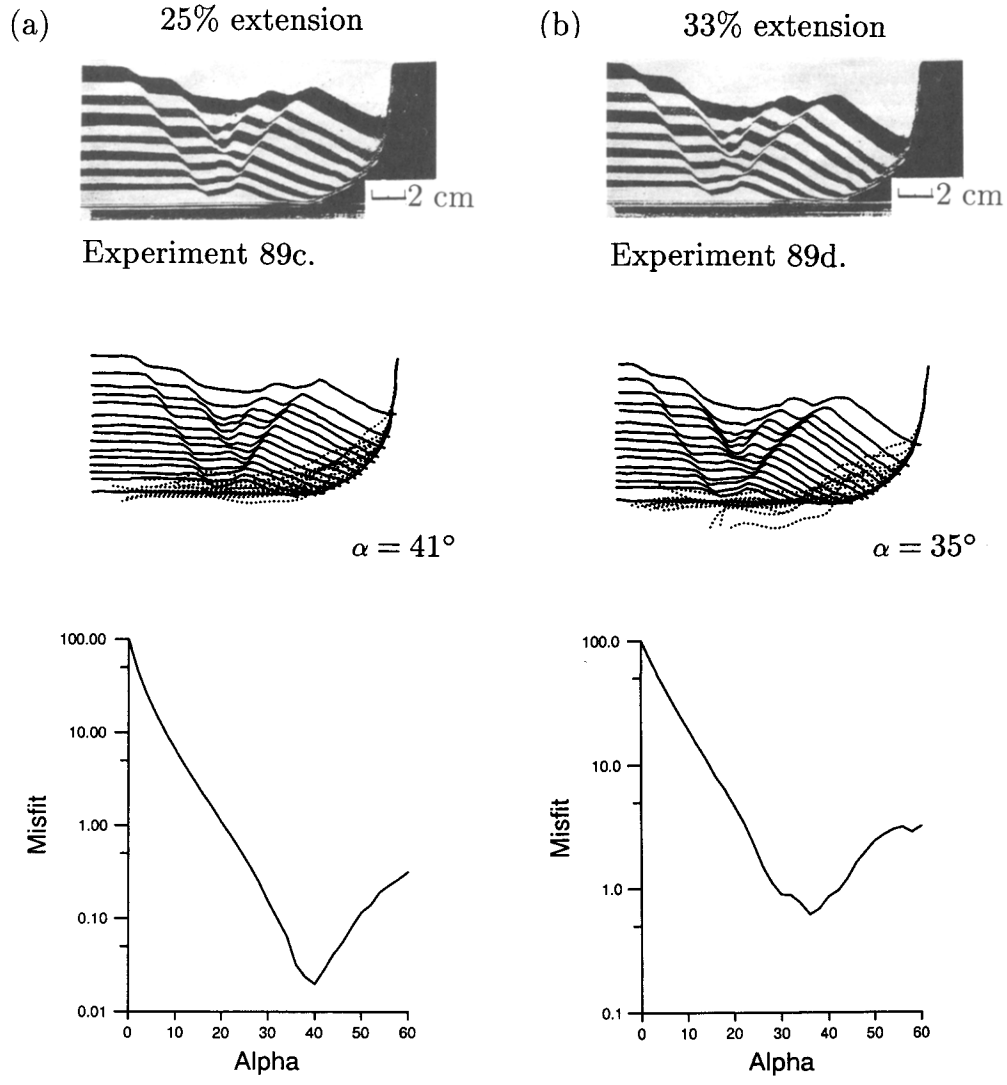

Fig. 9. (a) McClay & Ellis (1987, p. 122, fig. 6c. Experiment No. 89c) homogeneous sand layers. Reproduced with permission of Blackwell Scientific Publications Ltd. Inverse model and misfit function shown as before. Fourteen beds used. (b) McClay & Ellis (1987, p. 122, fig. 6d. Experiment No. 89d), homogeneous sand layers. Reproduced with permission of Blackwell Scientific Publications Ltd. Inverse model and misfit function shown as before. Fourteen beds used.

a scale similar to the model used in Fig. 4. $\mathcal{M}(\alpha, \phi_o, \lambda)$ is smooth and the location of the solution is equally dependent on α and ϕ_o. The fault in Fig. 5(b) has a length-scale 4 orders of magnitude smaller. Note that in this instance, the location of the solution is entirely controlled by the value of α. This result agrees with what one might have expected: the scale of the fault is considerably smaller than the compaction decay length and no compaction takes place even though there is a finite porosity of 40%. For comparison, a larger scale fault is shown in Fig. 5(c) (length scale greater than Fig. 5a by a factor of 5). In this case, $\mathcal{M}(\alpha, \phi_o, \lambda)$ looks very similar to that of Fig. 5(a) with ϕ_o and λ having slightly more control on the location of the solution.

LABORATORY-MODELLED FAULTS

Published laboratory models of normal faulting provide a useful means for testing kinematic methods such as that discussed here. The advantages of using these models are: (a) they are two-dimensional and the 'stratigraphy' is accurately known; (b) the fault geometry is known and does not change as deformation proceeds; (c) they are more realistic than synthetic examples and often show complex deformation.

Previously, it was argued that laboratory-modelled faults showed deformation which was more complex than planar bulk inclined simple shear (see e.g. Ellis & McClay 1988, Waltham 1989, 1990). The preliminary results of White (1992) suggested that this conclusion was overly pessimistic and that while the deformation is complex it could be adequately represented as bulk inclined simple shear. Here we test this assumption more rigorously by applying the revised inversion scheme to a large number of published laboratory-modelled faults.

All the laboratory models presented here come from McClay & Ellis (1987) and Ellis & McClay (1988). In each case, digitized hanging wall horizons were used to calculate function $\mathcal{M}$ and hence constrain the fault geometry at depth. Since the laboratory models were small

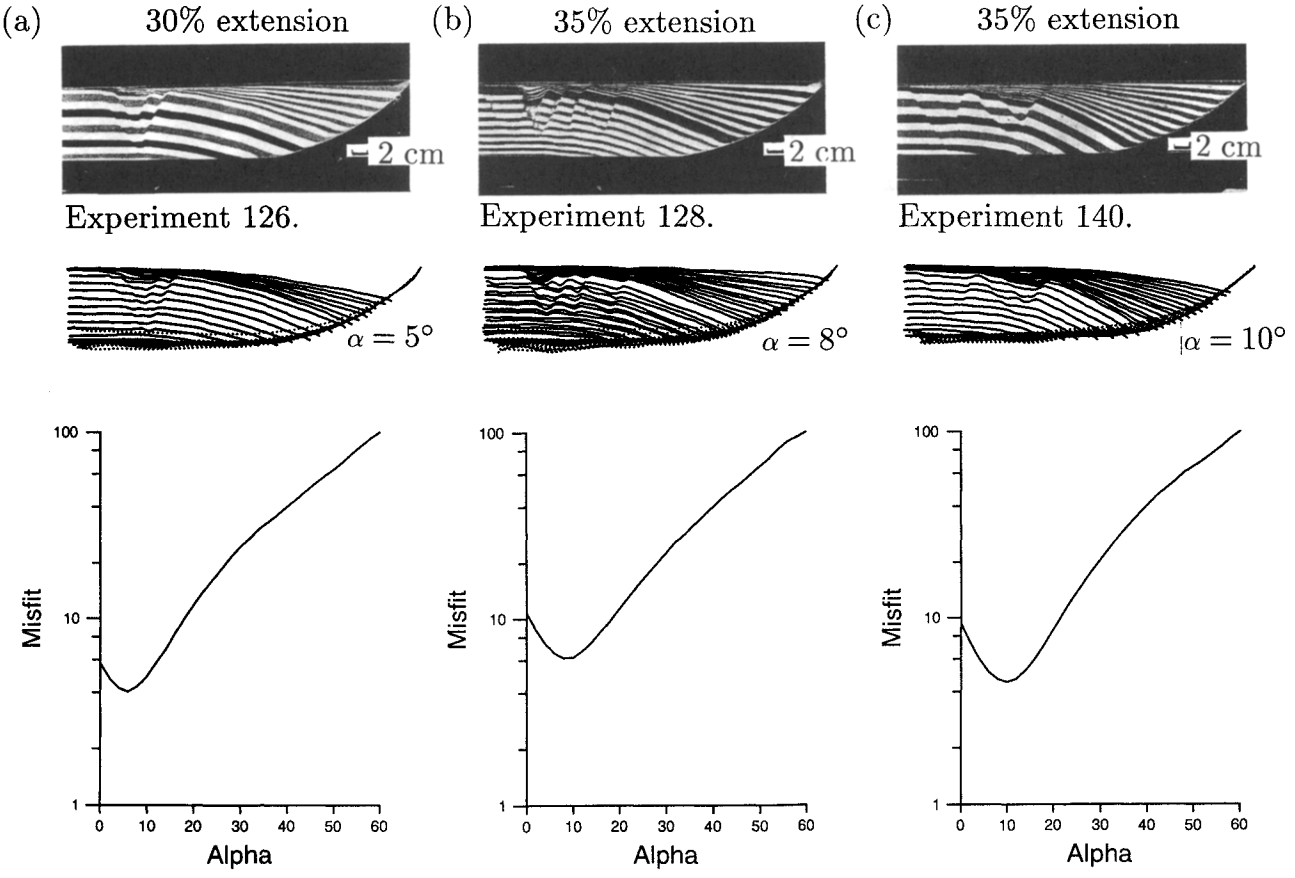

Fig. 10. (a) Ellis & McClay (1988, p. 61, fig. 10a. Experiment No. 126) homogeneous sand layers. Reproduced with permission of Blackwell Scientific Publications Ltd. Inverse model and misfit function shown as before. Seventeen beds used. (b) Ellis & McClay (1988, p. 62, fig. 11a. Experiment No. 128), alternate sand and clay layers. Reproduced with permission of Blackwell Scientific Publications Ltd. Inverse model and misfit function shown as before. Twenty-eight beds used. (c) Ellis & McClay (1988, p. 62, fig. 12a. Experiment No. 140, alternate mica and sand layers. Reproduced with permission of Blackwell Scientific Publications Ltd. Inverse model and misfit function shown as before. Twenty-three beds used.

scale (no greater than 15 cm high) compaction did not have significant effect on the deformation of the hanging wall horizons. Hence parameters ϕ_0 and λ were omitted from the inversion scheme. In each example $\mathcal{M}(\alpha)$ is normalized to 100 and plotted on a logarithmic scale against α.

Example 1

The first example (Figs. 6 and 7) consists of a series of three experiments. Each of the experiments represents the progressive extension across a single dog-leg fault of homogeneous sand layers which were horizontal prior to extension. In Fig. 6(a) 7.5% extension had occurred, 15% in Fig. 7(a), and 25% in Fig. 7(d).

The graphs of $\log_{10} \mathcal{M}$ vs α (Figs. 6e and 7c & f) indicate a minimum at $\alpha = 28°$ for the first experiment, at $\alpha = 31°$ in the second experiment, and at $\alpha = 31°$ in the final experiment. The faults calculated at the values of α indicated by the minimum of $\mathcal{M}(\alpha)$ are shown in Figs. 6(c) and 7(b) & (e). In both Figs. 7(b) & (e) the calculated faults are close to each other and match the fault used in the laboratory model well. In Fig. 6(c) the predicted faults are more widely spread and match the actual fault less well. We think that this relatively poor solution is a result of the very small amount of extension. However, compared with the predicted faults from the 'Chevron construction' (Verrall 1981), shown in Fig. 6(b), it is apparent that our solution is significantly better. Note also that the predicted faults from the 'Chevron construction' are widely spaced resulting in a high value of misfit indicated on the graph. A large value of misfit also occurs at $\alpha = 60°$: the actual faults which are predicted from the hanging wall horizons at this value of α are shown in Fig. 6(d). Note that the calculated areal difference between the predicted faults at $\alpha = 60°$ is lower than at $\alpha = 28°$. Therefore, for the reasons discussed previously, if the inversion had been based on areal difference instead of $\mathcal{M}(\alpha)$, the wrong solution would have been obtained.

The inversion had been applied previously by White (1992) to the five uppermost beds in the second experiment. The misfit between the predicted faults was not evaluated but estimated by trial and error. The estimated minimum misfit was at $\alpha = 33°$, which is close to the value of 31° we have now calculated from all the beds, White (1992) also showed that the inclusion of an initial porosity (ϕ_0) resulted in the prediction of different faults than when ϕ_0 was set at zero. As emphasized already, owing to the small size of the laboratory models, compaction had no effect on the deformation of the hanging wall horizons. Therefore a fault calculated from a horizon when $\phi_0 = 0\%$ should be the same as when ϕ_0 is non-zero. White (1992) obtained a differ-

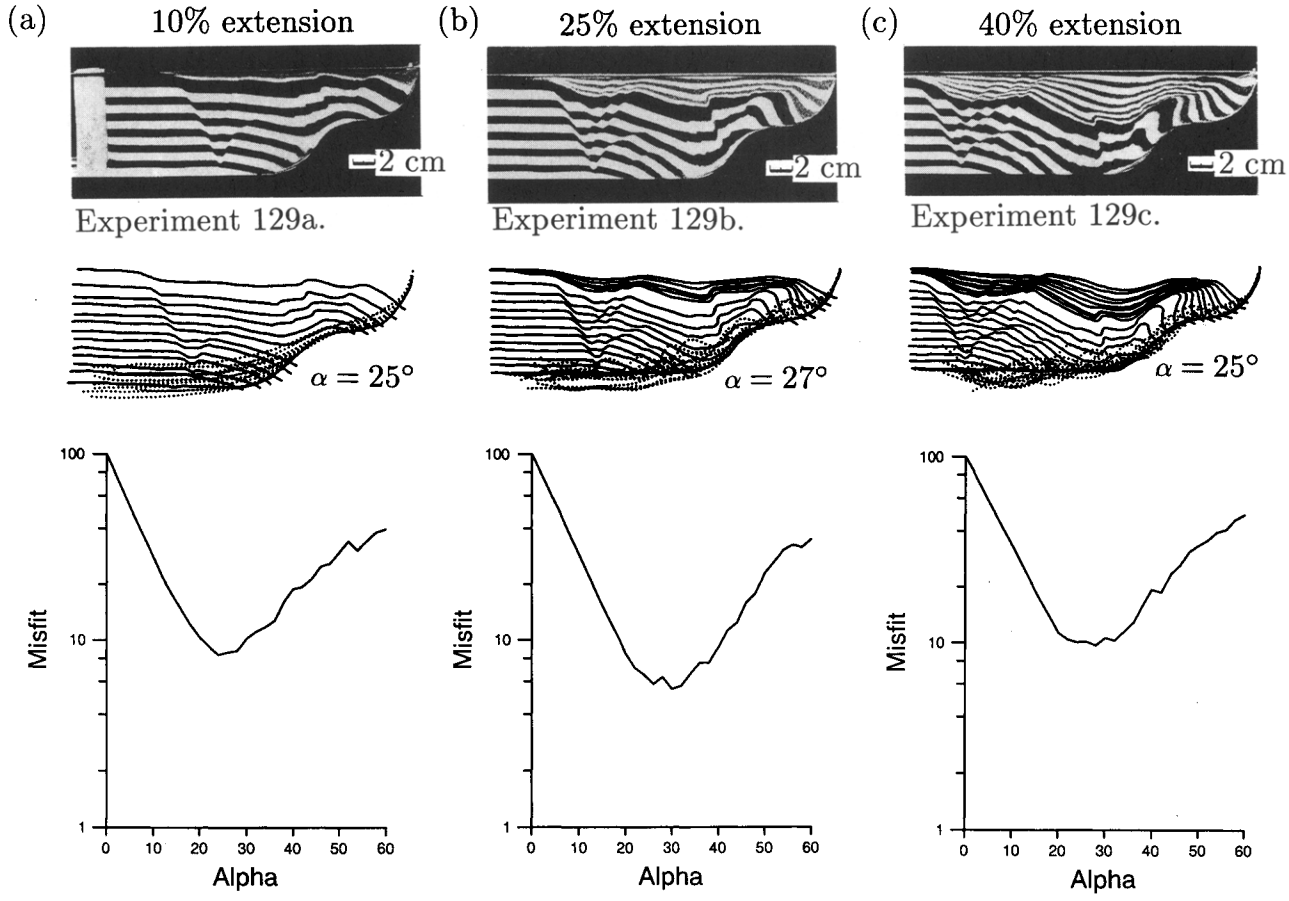

Fig. 11. (a) Ellis & McClay (1988, p. 63, fig. 14a. Experiment No. 129a), homogeneous sand layers. Reproduced with permission of Blackwell Scientific Publications Ltd. Inverse model and misfit function shown as before. Twelve beds used. (b) Ellis & McClay (1988, p. 63, fig. 14b. Experiment No. 129b), homogeneous sand layers. Reproduced with permission of Blackwell Scientific Publications Ltd. Inverse model and misfit function shown as before. Sixteen beds used. (c) Ellis & McClay (1988, p. 63, fig. 14c. Experiment No. 129c), homogeneous sand layers. Reproduced with permission of Blackwell Scientific Publications Ltd. Inverse model and misfit function shown as before. Twenty beds used.

ence due to scaling problems: depths of burial, z in equation (1), were measured in kilometres instead of centimetres. The same scaling problem is apparent in all of the laboratory examples used in that paper.

White *et al.* (1986) point out that there are important implications for the amount of extension that actually occurs if the hanging wall deforms by positively inclined simple shear. They show that the true extension, ε, is related to the apparent extension or heave, h, by

$$\varepsilon = h(1 + \tan\theta \tan\alpha), \quad (5)$$

where θ is the average dip of the main fault between the regional level and the point where the deformed bed meets the fault. The result of calculating the true extension for each of the beds in the third experiment is shown in Fig. 7(g). The amount of extension which actually took place in the experiment was 25%. The calculated extension for each of the beds is close to 25%. Similar results have been obtained for the other laboratory-modelled faults.

Example 2

The experiments in this example (Figs. 8 and 9) have a more rounded fault geometry than in Example 1. The hanging wall block immediately adjacent to the footwall appeared to have deformed by a rigid rotation rather than by simple shear. Therefore, it was anticipated that the inversion scheme, which assumes that deformation is solely by simple shear, would not be successful in predicting the correct fault from the deformed hanging wall horizons. However, in each case the minimum value of $\mathcal{M}(\alpha)$ calculated from the horizons coincided with a value of α which predicts faults fairly close to the real fault. The greatest difference between the predicted faults and the real faults is observed in the rotated region.

As in Example 1, the difference between the actual and predicted faults in the first experiment (Fig. 8a) was greater than in subsequent experiments (Figs. 8b and 9a & b). Therefore it appears that simple shear represented deformation of the hanging wall better when there has been extension of more than 7.5%.

Example 3

In each of the experiments shown in Fig. 10 a different hanging wall fill has been used with the same fault shape. The fault in each case is listric with a dip of 45° at the surface.

The first experiment (Fig. 10a) has a hanging wall fill of homogeneous sand. The horizons at the bottom of the

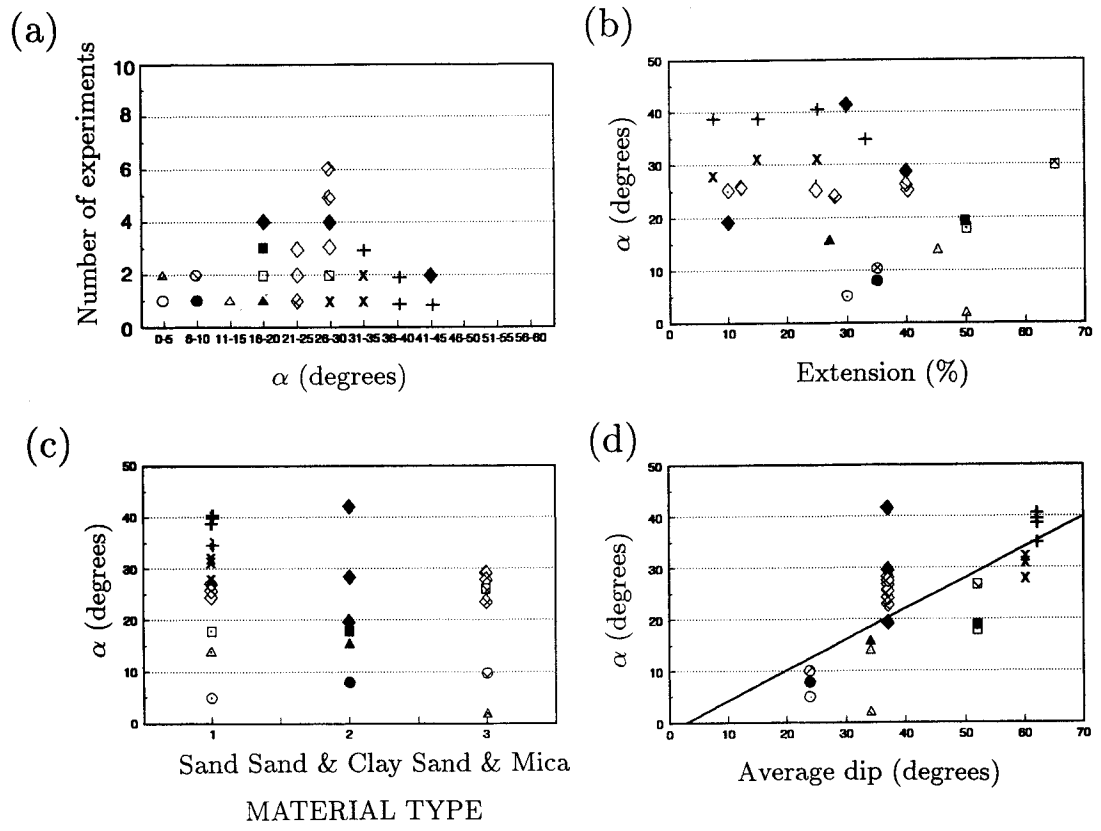

Fig. 12. Summary of results. Shape of symbol indicates geometry of normal fault used in experiment: × = planar dog-leg (60° average dip of main fault); + = listric (62° average dip of main fault); ○ = listric (24° average dip of main fault): △ = listric (34° average dip of main fault); □ = listric (52° average dip of main fault); ◇ = ramp–flat (38° average dip of main fault). Shading of symbol indicates composition of hanging wall fill: open = homogeneous sand; solid = alternate sand and clay layers; hatched = alternate sand and mica layers. (a) Number of experiments for each value of α. (b) Relationship between α and degree of extension. (c) Relationship between α and material used in hanging wall fill. (d) Relationship between α and average dip of main fault surface (see Table 1).

Table 1. Summary of results

Experiment No.	Composition of hanging wall	Extension (%)	Average dip of main fault (°)	α (°)
93a	Homogeneous sand	7.5	60	28
93b	Homogeneous sand	15	60	31
93c	Homogeneous sand	25	60	31
89a	Homogeneous sand	7.5	62	39
89b	Homogeneous sand	15	62	39
89c	Homogeneous sand	25	62	41
89d	Homogeneous sand	33	62	35
126	Homogeneous sand	30	24	5
128	Sand and clay	35	24	8
140	Sand and mica	35	24	10
125	Homogeneous sand	45	34	14
116	Sand and clay	27	34	16
139	Sand and mica	50	34	2
124	Homogeneous sand	50	52	18
143	Sand and clay	50	52	18
133	Sand and mica	65	52	27
129a	Homogeneous sand	10	38	25
129b	Homogeneous sand	25	38	27
129c	Homogeneous sand	40	38	25
131a	Sand and clay	10	38	24
131b	Sand and clay	30	38	26
131c	Sand and clay	40	38	27
119a	Sand and mica	12	38	19
119b	Sand and mica	28	38	42
119c	Sand and mica	40	38	28

section were laid down prior to extension whereas the upper horizons were deposited during extension, and as such represent syn-rift sediments. Both the pre-rift and syn-rift horizons were included in the inversion scheme. The faults predicted from the horizons, with α set at the value corresponding to the minimum of $\mathcal{M}(\alpha)$, closely match the actual fault.

In the next experiment, the hanging wall fill was changed from homogeneous sand to alternate layers of sand and clay (Fig. 10b). The use of alternate sand and clay layers introduced a competency contrast between the layers (Ellis & McClay 1988). Function $\mathcal{M}(\alpha)$ has a unique minimum at α equal to 8° and the predicted faults at this value of α match the actual fault very well. Consequently, even with the introduction of a competency contrast between the layers, deformation of the hanging wall was represented adequately by bulk simple shear.

The hanging wall fill in the final experiment consisted of alternate layers of sand and mica (Fig. 10c). Mica flakes parallel to bedding should produce anisotropy between the layers. Subsequently, extension was expected to have been accommodated by some degree of bedding-parallel slip (Ellis & McClay 1988) rather than by bulk simple shear alone. However, the predicted faults at the value of α indicated by the minimum value of $\mathcal{M}(\alpha)$ all match the real fault closely. Therefore, although some inter-bed slip may have occurred, the average deformation of the hanging wall can still be adequately modelled by bulk inclined simple shear.

Example 4

The ramp–flat fault geometry was used in each of the laboratory experiments shown in Fig. 11. Each of the experiments represents the progressive extension from the fault surface of layers of homogeneous sand. The faults predicted from the value of α indicated by the minimum of $\mathcal{M}(\alpha)$ match the actual fault reasonably well. Hence, even when complex fault geometries are used, bulk simple shear is an adequate kinematic approximation of the deformation.

Summary

The results of Figs. 6–11 in addition to the results of inverting other laboratory models published in McClay & Ellis (1987) and Ellis & McClay (1988) are summarized in Fig. 12 and in Table 1. Obviously, it is difficult to draw firm conclusions from a relatively small body of laboratory models. Therefore our results should be treated with some caution. To gain a better understanding of why hanging wall deformation can be represented by a specific angle of bulk simple shear it would be necessary to complete many more experiments and apply statistical analysis to the results.

Each laboratory model is labelled according to the average dip of the main fault and the hanging wall fill used (see Caption to Fig. 12 for detailed explanation). A total of 25 experiments were inverted, and in 16 cases α was between 15° and 35° (Fig. 12a). In all cases α was less than 45°.

Figure 12(b) shows α as a function of extension. In general, as the amount of extension increases, α stays approximately constant indicating that the orientation of the shear planes along which deformation is imagined to have occurred remains the same throughout the period of extension. The composition of the hanging wall fill has little effect on α (Fig. 12c). Models where the same fault shape and varying hanging wall fills are used, results in approximately the same value of α.

Finally, α is plotted as a function of average dip of the main fault surface (Fig. 12d). It is clear that fault shape is important in determining the value of α. A general relationship is apparent: higher values of main fault average dip result in higher values of α. The dynamic reason for the relationship and indeed why hanging wall deformation can be generalized by bulk inclined simple shear is not readily apparent from the kinematic model.

CONCLUSIONS AND FURTHER WORK

This paper builds on the preliminary results presented by White (1992). The most important conclusion is that, despite the fact that hanging wall deformation is often complex, it can be represented as arbitrarily inclined bulk simple shear. It must be emphasized that planar simple shear may not be clearly apparent since it only represents the bulk or average deformation: the vorticity caused by bulk simple shear can introduce local complexity in the form of small-scale rotation and synthetic faulting. Note also that bulk inclined simple shear does not preclude the existence of local flexural-slip (Davison 1986, Higgs *et al.* 1991).

The method has been tested in two ways. Firstly, synthetic hanging wall stratigraphy generated by forward modelling was used to check the algorithm and to examine the shape of misfit function, $\mathcal{M}(\alpha, \phi_o, \lambda)$. $\mathcal{M}$ is shown to be a more appropriate method of measuring misfit than areal difference which was used previously. It varies smoothly and has a global minimum, thus indicating that unique solutions can be obtained. The inversion scheme was successfully automated to find the global minimum without having to sample α–ϕ_o–λ space completely. The method used to find the global minimum was the modified Powell's Method (Press *et al.* 1986).

The method has been tested on large numbers of published two-dimensional laboratory experiments. In each case, as many hanging wall horizons as possible are used in the inversion scheme. The results are encouraging and suggest, at this stage, that the underlying fault geometry rather than either the degree of extension or the composition of the hanging wall fill, is the main control on the value of α. Higher values of α result from higher values of average main fault dip.

One of the most important features of the scheme is

that large amounts of hanging wall information are used to constrain the fault geometry at depth. This approach has two advantages. First it gives confidence in the result, and secondly if no solution is found, inferences may be drawn concerning the underlying assumptions (i.e. the fault shape may have altered during deformation or perhaps there is displacement out of the plane of the section). Other inversion schemes which use the geometry of a single hanging wall horizon are less useful in this regard.

A major assumption made in the inversion scheme is that all the deformation occurs within the plane of the section. For two-dimensional laboratory-modelled faults this assumption is valid, but in general for normal faults in extensional sedimentary basins, this assumption is likely to be incorrect. Hence a generalized three-dimensional model which includes an additional parameter of oblique extension within the horizontal plane is being developed. At present, it is not clear how important oblique horizontal extension in three-dimensions will be in affecting the calculated fault geometry. It may well turn out that in most circumstances two-dimensional modelling is adequate. However until careful testing is completed we will not know for certain.

Acknowledgements—H. G. Kerr gratefully acknowledges a Petroleum Science and Technology Institute (P.S.T.I.) studentship. P.S.T.I. also provided the computational facilities. We thank E. D. Kerr and S. Singh for their assistance. D. Waltham and G. Yielding provided very helpful reviews. Petroleum Science and Technology Institute Contribution No. 006 and Department of Earth Sciences Contribution No. 2302.

REFERENCES

Davison, I. 1986. Listric normal fault profiles: calculation using bed-length balance and fault displacement. *J. Struct. Geol.* **8**, 209–210.

Ellis, P. G. & McClay, K. R. 1988. Listric extensional fault systems—results of analogue model experiments. *Basin Res.* **1**, 55–70.

Faure, J.-L. & Chermette, J.-C. 1989. Deformation of tilted blocks, consequences on block geometry and extension measurements. *Bull. Soc. geol. Fr.* **8**, 209–210.

Gibbs, A. D. 1983. Balanced cross-section construction from seismic sections in areas of extensional tectonics. *J. Struct. Geol.* **5**, 153–160.

Groshong, R. H., Jr. 1989. Unique determination of normal fault shape from hanging wall bed geometry in detached half grabens. *Eclog. geol. Helv.* **83**, 455–471.

Higgs, W. G., Williams, G. D. & Powell, C. M. 1991. Evidence for flexural shear folding associated with extensional faults. *Bull. geol. Soc. Am.* **103**, 710–717.

Jackson, M. & Galloway, W. 1984. Structural and depositional styles of Gulf coast Tertiary continental margins: application to hydrocarbon exploration. *Am. Ass. Petrol. Geol. Education Course Notes* **25**.

Kligfield, R., Crespi, J., Naruk, S. & Davis, G. H. 1984. Displacement and strain patterns of extensional orogens. *Tectonics* **3**, 577–609.

McClay, K. R. & Ellis, P. G. 1987. Analogue models of extensional fault geometries. In: *Continental Extensional Tectonics* (edited by Coward, M. P., Dewey & Hancock, P. L.). *Spec. Publs geol. Soc. Lond.* **28**, 109–125.

Nunns, A. G. 1991. Structural restoration of seismic and geologic sections in extensional regimes. *Bull. Am. Ass. Petrol. Geol.* **75**, 278–297.

Press, W. H., Flannery, B. P., Teukolsky, S. A. & Vetterling, W. T. 1986. *Numerical Recipes: The Art of Scientific Computing*. Cambridge University Press, Cambridge, 294–301.

Roberts, A. G., Yielding, G. & Freeman, B. 1990. The geometry of normal faults. *J. geol. Soc. Lond.* **147**, 185–187.

Rowan, M. G. & Kligfield, R. 1989. Cross-section restoration and balancing as aid to seismic interpretation in extensional terranes. *Bull. Am. Ass. Petrol. Geol.* **73**, 955–966.

Sclater, J. G. & Christie, P. A. F. 1980. Continental stretching: an explanation of the post-mid Cretaceous subsidence of the Central North Sea Basin. *J. geophys. Res.* **85**, 3711–3739.

Suppe, J. 1983. The geometry and kinematics of fault bend folding. *Am. J. Sci.* **283**, 684–721.

Verrall, P. 1981. *Structural Interpretation with Applications to North Sea Problems*. Course Notes No. 3, Joint Association for Petroleum Exploration Courses (U.K.).

Waltham, D. 1989. Finite difference modelling of hanging wall deformation. *J. Struct. Geol.* **11**, 433–437.

Waltham, D. 1990. Finite difference modelling of sand-box analogues, compaction and detachment-free deformation. *J. Struct. Geol.* **12**, 375–381.

White, N. 1987. Constraints on the measurement of extension in the brittle upper crust. *Norsk. geol. Tidsskr.* **67**, 269–279.

White, N. 1992. Determining normal fault geometry. *J. geophys. Res.* **97**, 1715–1733.

White, N., Jackson, J. A. & McKenzie, D. P. 1986. The relationship between the geometry of normal faults and that of the sedimentary layers in their hanging walls. *J. Struct. Geol.* **8**, 879–909.

White, N. & Yielding, G. 1991. Calculating normal fault geometries at depth: theory and examples. In: *The Geometry of Normal Faults* (edited by Roberts, A. M., Yielding, G. & Freeman, B.). *Spec. Publs geol. Soc. Lond.* **56**, 251–260.

Williams, G. & Vann, I. 1987. The geometry of listric normal faults and deformation in their hanging walls. *J. Struct. Geol.* **9**, 789–795.